Asociación Argentina
de Mecánica Computacional

Mecánica Computacional Vol XXIX, págs. 6149-6161 (artículo completo)
Eduardo Dvorkin, Marcela Goldschmit, Mario Storti (Eds.)
Buenos Aires, Argentina, 15-18 Noviembre 2010

ERROR ANALYSIS OF THE DIGITAL IMAGE CORRELATION METHOD

Jakson M. Vassoler[a] **and Eduardo A. Fancello**[a]

[a]*Departamento de Engenharia Mecânica, Universidade Federal de Santa Catarina, Campus Universitário, Trindade, 88040-970 Florianópolis, SC, Brasil.* *http://www.grante.ufsc.br*

Keywords: Digital Image Correlation, Displacement measurement, Measurement errors.

Abstract. The optical method Digital Image Correlation (DIC) has been extensively studied due its capability to measure the entire displacement field over a body surface. This particular feature makes this measurement method appropriated to measure heterogeneous displacement fields in large strains. Then, it can be applied for specimens used in standard tests or even for in vivo applications, like biological tissues. In the last years, many works about the performance of different DIC algorithms were published. These studies demonstrated the excellent accuracy and precision of the optical method; however almost all have been focused on the measurement errors for low order displacement fields, like translation and constant strain, and only a few works have been studied the error related to high-order displacement fields. Since this method shown great applicability for heterogeneous displacement fields founded in large strains, this work investigates the displacement measure accuracy for different possible sets of the DIC algorithm using numerically simulated images for zero, first and second order displacement fields in order to consider only errors related to the algorithm. The results shown that the accuracy may vary in many orders of magnitude from the choice of different setups, where the relation between the subset size and the speckle granule size is quite important.

1 INTRODUCTION

The identification of constitutive model parameters requires experimental tests to provide information about the mechanical behavior of materials. Traditional experimental tests based on contact-techniques have limitations to generate appropriated data for complex heterogeneous displacements fields, like the necking phenomenon. These methods are limited to measure localized strains in the contact points and then the measuring may not be able to represent the mechanical behavior over the entire specimen in large deformations. During years the optical method Digital Image Correlation (DIC) has been extensively investigated and improved to achieve high accuracy, (Bruck et al., 1989), (Vendroux and Knauss, 1998), (Lu and Cary, 2000), (Sutton et al., 2000), (Bing et al., 2006), (Pan et al., 2008), (Pan et al., 2009a) and (Pan et al., 2010). Its main characteristic is the capability to measure the entire displacement field of the specimen surface for a wide range of displacement magnitudes. Many applications for different materials are reported in literature. In (Vanlanduit et al., 2009) the DIC technique is used to monitor the crack growth process on an aluminum U-profile during a cyclic fatigue test. The displacement accuracy reported is a few hundredths pixels. In (Tao and Xia, 2005) is presented a multiaxial cyclic/fatigue test for an epoxy polymer. In (Guastavino and Göransson, 2007) the three-dimensional displacement over the surface of anisotropic porous cellular melamine foam was measured by the DIC method in order to capture the effects of viscoelasticity in the polymer. The optical method was employed in (Zhang and Arola, 2004) to determine the elastic modulus and the Poisson's ratio of arterial and dermal tissue. Also in (Zhang and Arola, 2004) was measured the relative displacement between bone/bone cement and bone cement/prosthesis interface. The results of this study had shown the possibility to use the DIC method for in vivo applications. In the works reported above the displacement field is quite complex and very difficult to be measured by a traditional contact-technique, like strain-gauge or clip-gauge.

An important issue about the DIC technique is accuracy. Although originally restricted to the size of one-pixel, different algorithms called sub-pixel techniques, has been proposed and used to improve DIC accuracy. In (Bing et al., 2006) the performance of three most used sub-pixel techniques were compared for simulated images. These techniques are known as Curve-fitting, Gradient-based and Newton-Raphson algorithms. The last two cases are based on the identification of the parameters that define the mapping of a subset of pixels in order to maximize the image correlation. The results show that the Newton-Raphson approach is the more accurate and stable. Other interesting approaches like the use of genetic algorithms, finite elements and B-splines are reported in (Pan et al., 2009b) but it appear to have a lower performance than the so called Newton-Raphson technique in terms of accuracy.

Besides the choice of the algorithm, other factors influence the accuracy of the DIC method. The measurement errors may be classified in two types: errors associated to the experimental setup (acquisition system, illumination conditions) and errors associated to the correlation algorithm. The experimental errors are related basically to the variations of illumination and the quality of the acquisition system, i.e., the noise during the acquisition and digitalization, the imaging distortion, position of the camera respect to the specimen, etc. The errors related to the algorithm are due to different choices of the implementation of the algorithm, i.e., the choice of the subset size, correlation function, sub-pixel algorithm, shape function and interpolation scheme. Here, the error due to the speckle pattern is considered to be an algorithm error because it changes significantly the measurement accuracy of the algorithms. Despite many works on DIC are found in literature, only a few of them deal with the errors related to the correlation algorithm. In (Pan et al., 2009b) the errors related to the specimen, loading, imaging and cor-

relation algorithm are discussed. A study of the systematic errors due to use of shape functions of lower order than the displacement field is presented in (Schreier and Sutton, 2002). Also, in (Schreier and Sutton, 2002) it is presented some requirements about properties of the pattern, subset size and order of the shape functions. In (Lecompte et al., 2006) is presented a study about the relation between the mean speckle size and the subset size. To this aim, a reference image was acquired from a randomly sprayed white flat surface and then numerically stretched by two deformations (homogeneous and non homogeneous) obtained from finite element simulations. The use of numerically stretched images is usually chosen in order to eliminate errors caused by the acquisition system, imperfect loading, out-of-plane motion and illumination fluctuation. In the works (Bing et al., 2006), (Pan et al., 2010) and (Schreier and Sutton, 2002) the authors decided to use Fourier domain shifting to offset the pixels to non-integer positions. Although this approach seems to be more accurate to create stretched images, it is not able to impose localized high-order displacement fields like those obtained by FEM simulations in (Lecompte et al., 2006). In (Pan et al., 2010) the author proposes the Mean intensity gradient to obtain the optimal subset size, where it is used the Newton-Raphson algorithm, the simplest correlation coeficient and the zero-order shape function for pure in-plane translation tests. In (Sutton et al., 2009) it is presented a method to estimate an appropriated pattern density for different subset sizes determining the characteristic sampling length of the speckle granules.

The main objective of the present work is to investigate the accuracy of the displacement measurements associated exclusively to the correlation algorithm for different possible sets of image speckle, subset size and interpolation functions. The errors related to the acquisition system are automatically excluded of this study since the sequences of speckle images are numerically simulated.

2 DIGITAL IMAGE CORRELATION ALGORITHM

In order to define a common notation, it follows a brief description of the subset-based digital image correlation procedure used in this work. A virtual grid of evenly spaced points, called markers, is defined on the studied region of the reference image. Also, a square area of pixels around each marker, called subset, is defined. The digital image correlation algorithm tracks the displacements of the markers in the sequence of digital images acquired in experimental tests. The method searches for the best correspondence between the square area of the subset in the reference image and the square area in a subsequent image. Being the marker the geometric center of the subset, this last provides sufficient information to the tracking algorithm in order to obtain a unique and truthful correlation. The cross-correlation between reference and subsequent subsets of $(2M+1) \times (2M+1)$ pixels is based on the Zero-mean Normalized Sum of Squared Differences (ZNSSD) correlation coefficient:

$$C_{ZNSSD} = \sum_{i=-M}^{M} \sum_{i=-M}^{M} \left[\frac{f(x,y) - f_m}{\sqrt{\sum_{i=-M}^{M} \sum_{i=-M}^{M} (f(x,y) - f_m)^2}} - \frac{g(x',y') - g_m}{\sqrt{\sum_{i=-M}^{M} \sum_{i=-M}^{M} (g(x',y') - g_m)^2}} \right]^2 \tag{1}$$

where $f(x,y)$ is the gray intensity at coordinates (x,y) in the reference image (undeformed), $g(x',y')$ is the gray intensity at coordinates (x',y') in the deformed image and

$$f_m = \frac{1}{2M+1}\sum_{i=-M}^{M}\sum_{i=-M}^{M} f(x,y),$$
$$g_m = \frac{1}{2M+1}\sum_{i=-M}^{M}\sum_{i=-M}^{M} g(x',y'). \tag{2}$$

are, respectively, the mean gray values in the reference and deformed subsets. The ZNSSD correlation coefficient is insensitive to the offset and linear scale of illumination intensity offering a robust noise-proof performance (Pan et al., 2009b).

In order to allow the deformation of the subset and therefore improving the correlation, different shape functions (mapping functions) may be used. In the present work, the reference subset is mapped to the target subset by a second-order mapping function:

$$x' = x + \bar{u} = x + u + u_x\triangle x + u_y\triangle y + u_{xy}\triangle x\triangle y + u_{xx}\triangle x^2 + u_{yy}\triangle y^2,$$
$$y' = y + \bar{v} = y + v + v_x\triangle x + v_y\triangle y + v_{xy}\triangle x\triangle y + v_{xx}\triangle x^2 + v_{yy}\triangle y^2. \tag{3}$$

where u and v are respectively the $x-$ and $y-$directional displacement components of the reference subset center, u_x, u_y, v_x, v_y are the first-order displacement gradients and u_{xx}, u_{xy}, u_{yy}, v_{xx}, v_{xy}, v_{yy} are the second-order displacement gradients. This mapping function is much more computationally expensive (12 parameters) than a simpler first-order function (6 parameters) which can be obtained eliminating the last three terms of each expression (Schreier and Sutton, 2002). However, the quadratic terms allows the use of a larger subset area with accurate measurement for high-order displacement fields. However, since the image processing is performed off-line (no real-time processing), requirements of computational performance may be taken as a second concern. The algorithm minimizes the ZNSSD correlation coefficient C_{ZNSSD}, solving a set of twelve non-linear functions, where the minimizing arguments, solution of the minimum problem, correspond to the unknown parameters

$$\mathbf{p} = \left[\begin{array}{cccccccccccc} u & v & u_x & v_x & u_y & v_y & u_{xx} & v_{xx} & u_{xy} & v_{xy} & u_{yy} & u_{yy} \end{array}\right]. \tag{4}$$

The set of equations is solved using the iterative Newton-Raphson procedure:

$$\mathbf{p} = \mathbf{p}_0 - \frac{\nabla C_{ZNSSD}(\mathbf{p}_0)}{\nabla\nabla C_{ZNSSD}(\mathbf{p}_0)}. \tag{5}$$

where $\mathbf{p}_0$ is the initial values of the solution and ∇C_{ZNSSD} and $\nabla\nabla C_{ZNSSD}$ are, respectively, the first and second-order derivatives of the correlation coefficient respect to the unknown parameters $\mathbf{p}$.

This algorithm is highly recommended for practical use due to its higher accuracy, stability and application (Bing et al., 2006). More details about this digital image correlation algorithm and shape functions can be found in the works (Pan et al., 2009b) and (Pan et al., 2010).

2.1 Sub-pixel Interpolation

In a real problem the pixel can be offset to non-integer position (x',y'). The sub-pixel interpolation procedures seek for these offsets even having integer information in the images. To

this aim, an interpolation scheme has to be used to reconstruct the gray intensity value $g(x', y')$ at the deformed position. It is known that that spline interpolators have been quite successful in this task. (Schreier et al., 2000) investigated bi-cubic polynomial interpolation, B-spline interpolation and bi-quintic spline interpolation. It was concluded that the mean systematic error of splines has the same periodic shape with different amplitudes and the amplitude decrease for high-order splines, that are highly recommended. In this work the high-order bi-cubic spline interpolation is used.

2.2 Subset Size

The subset size determines the area around the marker that will be taking into account in the cross-correlation to obtain the marker displacement. This value is set up by the user and it can vary from a few pixels to a hundred pixels, choice that can change considerably the measuring accuracy. A small size is preferable due to low computational cost and it allows the use of a minor order of shape function even for complex displacements field. In the other hand, the subset size has to contain enough information (intensity pattern) to perform the cross-correlation and to obtain high accuracy. Then, an appropriated relation between the subset size and the speckle granules should be used. In this work, three different subset sizes are used: 21×21, 31×31, and 41×41.

3 SIMULATED SPECKLE IMAGES

In order to evaluate the displacement measure accuracy related only to the algorithm, the numerical simulated image data can not contain additional errors associated to the specimen, like acquiring system and noise. Again, numerical generation of different displacement fields can result in the offset of the pixels to non-integer positions. Thus, appropriated interpolation schemes must be employed. In (Schreier and Sutton, 2002) the discrete Fourier transform is used for each row of the image to avoid phase errors associated to polynomials or B-spline interpolators. In (Bing et al., 2006) a modified analytic expression of this interpolator is proposed in which the transformation is performed for each speckle granule, instead of each row of the image. In the present work, the deformed images are generated by using the expression proposed in (Bing et al., 2006). The deformed image I_n of a reference image I_1 is obtained by the expression

$$\begin{aligned} I_1 &= \sum_{k=1}^{s} I_0^k \exp\left(\frac{-\left((x-x_k)^2+(y-y_k)^2\right)}{R^2}\right), \\ I_n &= \sum_{k=1}^{s} I_0^k \exp\left(\frac{-\left((x-x_k-\bar{u})^2+(y-y_k-\bar{v})^2\right)}{R^2}\right) \end{aligned} \tag{6}$$

where I_0^k is the random peak intensity of each speckle granule, x_k and y_k are the positions of each speckle granule, s is the total number of speckle granule, R is the size of the speckle granule and $\bar{u}$ and $\bar{v}$ are the imposed displacements along the direction X and Y, respectively.

The systematic error associated to the algorithm is computed as the difference between the pre-imposed and the measured displacement:

$$e_s = \bar{u}_{imposed} - \bar{u}_{measured} \tag{7}$$

In the present study the sequence of images were numerically generated with different sizes of speckle granules presented in Tab. 1. These speckle distributions represent a speckle applied

over the specimen surface in a real experimental test, more information about requirements in the speckle pattern distribution, minimum subset size and minimum order of the shape functions, presented are studied can be found in (Schreier and Sutton, 2002) and (Pan et al., 2009b).

	s	R
Large speckle granule	1200	4
Median speckle granule	2500	2.5
Small speckle granule	5100	1

Table 1: Speckle granules characteristics of the generated images.

The reference images for the three different speckle granule size are shown in Fig. 1.

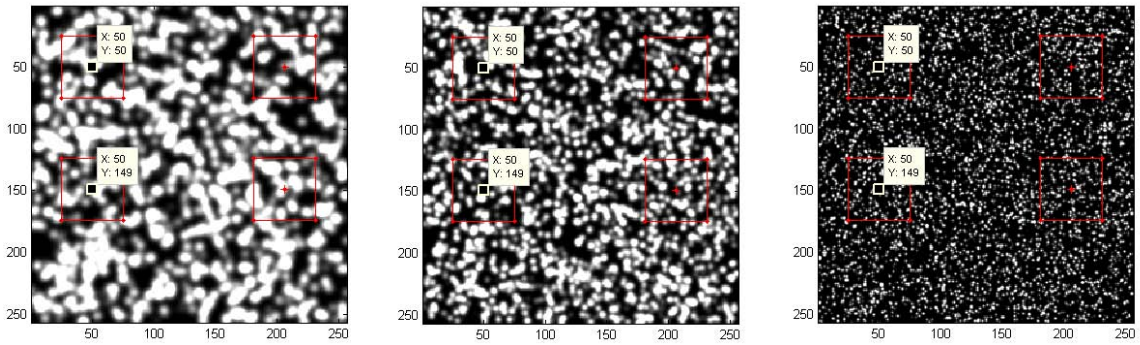

Figure 1: Undeformed images for the large, median and small speckle granule (left to right)

3.1 Type of Displacement Fields

Some authors have been studying the sub-pixel error for a constant displacement field (rigid translation) (Bing et al., 2006), (Pan et al., 2010) and (Schreier et al., 2000). A few studies have been performed about the error in high order displacement fields (Schreier and Sutton, 2002), (Lecompte et al., 2006), which it's quite common in heterogeneous strain. Since the algorithm has to be able to register sub-pixel displacements for complex displacement fields commonly found in uniaxial tests after necking, the measurement accuracy of the algorithms for high-order displacements fields should be widely investigated. In the present work sets of images containing 256 x 256 pixels were numerical generated for three different deformations: rigid translation, first-order displacement field and second-order displacement field. These displacement fields are defined for each deformation field and then they are substituted in 6 in order to produce the numerical generated images.

3.1.1 Rigid translation

In this case, the displacement field is defined by:

$$\begin{aligned} \bar{u}(x,y) &= 0 \\ \bar{v}(x,y) &= a \end{aligned} \tag{8}$$

This mapping was used to generate a sequence of 21 images with a homogeneous displacement over the entire image ranging from 0 to 1 pixel with a shift of $a = 0.05$ pixel. This displacement

field represents a rigid translation of the reference image and no strains are produced. The correlation analysis was performed using a square grid, with $47 \times 47 = 2209$ markers evenly spaced (of 4 pixels).

3.1.2 First-order displacement field

The linear displacement field is defined by:

$$\begin{aligned} \bar{u}(x,y) &= 0 \\ \bar{v}(x,y) &= ay \end{aligned} \tag{9}$$

A set of 11 images ranging from $a = 0$ to $a = 0.1$ is shifted of $a = 0.01$. This expression defines a nonhomogeneous displacement field over the images that correspond to deformed images with a homogeneous strain field. The last generated image ($a = 0.1$) represents 10% of strain and the images are shifted of 1% of strain ($a = 0.01$). A square grid with 44×53 markers (2332 points) evenly spaced of 3 pixels was analyzed.

3.1.3 Second-order displacement field

The second order displacement field was generated using the expression

$$\begin{aligned} \bar{u}(x,y) &= 0 \\ \bar{v}(x,y) &= ay^2 \end{aligned} \tag{10}$$

The second order coefficient is shifted of $a = 0.0001$. Eleven different values for a were used, ranging from 0 to 0.001. The grid of markers was composed with $34 \times 53 = 1802$ points, evenly spaced by 3 pixels.

The deformed images generate for this displacement field represent a nonhomogeneous displacement and strain field. The last deformed images for the three speckle granule sizes (Tab. 1) are shown in Fig. 2.

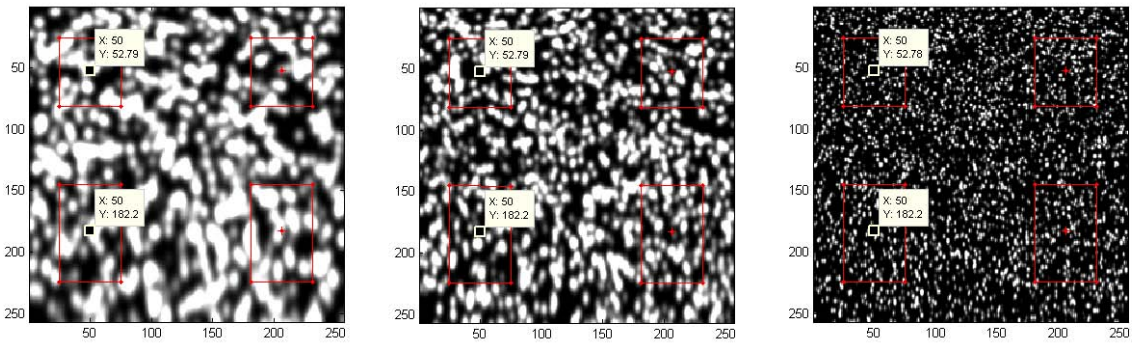

Figure 2: The second-order displacement field of the last deformed images for the large, median and small speckle granule (left to right)

4 ERROR ANALYSIS

In this section an error analysis of the correlation algorithm and its dependence on user setups like subset size and speckle granule size is performed. Systematic errors coming from image

acquisition are not expected, since the displacements fields tested were numerically generated as presented in the previous section.

The subset size and the speckle pattern influence significantly the accuracy of the measurement, since the error depends on the interpolation of the gray-values of the speckle pattern for non-integer position. If the speckle granules are large, the gray-value surface is smoother than a surface with speckle granules of a few pixels. In the other hand, the subset size changes the amount of interpolated pixels taken into account to approximate the shape function parameters. Then, different setups can lead to different results and appropriated subset size and speckle pattern are preferred to increase the accuracy in high-order displacement fields.

The DIC method allows to choose different setups of the algorithm in order to obtain the wanted accuracy. In the correlation algorithm was used the ZNSSD correlation coefficient with the second-order mapping function in order to capture appropriately high-order displacement fields and a high-order spline interpolator function to reduce phase errors of the sub-pixel measuring. At this point only the subset size has to be determined and it is related to the speckle granule size, that in its turn, it is related to the order of the displacement field.

The results for the three displacement fields of the three speckle granule sizes are presented for different subset sizes:

4.1 Rigid translation

The 21 generated images representing a progressive rigid translation from 0 to 1 pixel was used for error calculations. The error results are shown in Fig. 3. Each column represents the maximum absolute, mean and deviation error respectively, for three different granular sizes of the image pattern. Each graph includes the error curves for different subset sizes.

The image with large granular sizes presents a maximum absolute error along the y-direction of about 0.0012 pixels, the pattern with medium granular size presents an absolute error of about 0.009 pixels and the small granular size an absolute error of about 0.07 pixels using a subset size of 21×21 pixels.

The mean errors showed a sinusoidal shape with period of 1 pixel and no dependency on the subset size. In the other hand, the mean error changes significantly for different granular sizes. It is worth mentioning that the mean errors along the y-direction have the same period for different subset sizes and they are in phase because all the pixels in the reference image are offset by the same value. It should be noted that, for all cases, the absolute error of the three generated speckles pattern decrease when the subset size increases.

4.2 First-order displacement field

The first-order displacement field was analyzed up to 10% of stretching and the error results are shown in Fig. 4. As in the rigid translation, the pattern with small granular size showed, in general, larger errors than those obtained with the pattern with larger granules.

Again, the pattern with small granular size presents a maximum absolute error of about 0.00085 pixels. The medium pattern presents an absolute error of about 0.004 pixels while the small pattern presents an absolute error of about 0.087 pixels along the y-direction. The image compared used a subset size of 21×21 pixels.

It is also noted that the absolute error along the X and Y directions of the three generated speckles pattern decrease when the pattern size increases.

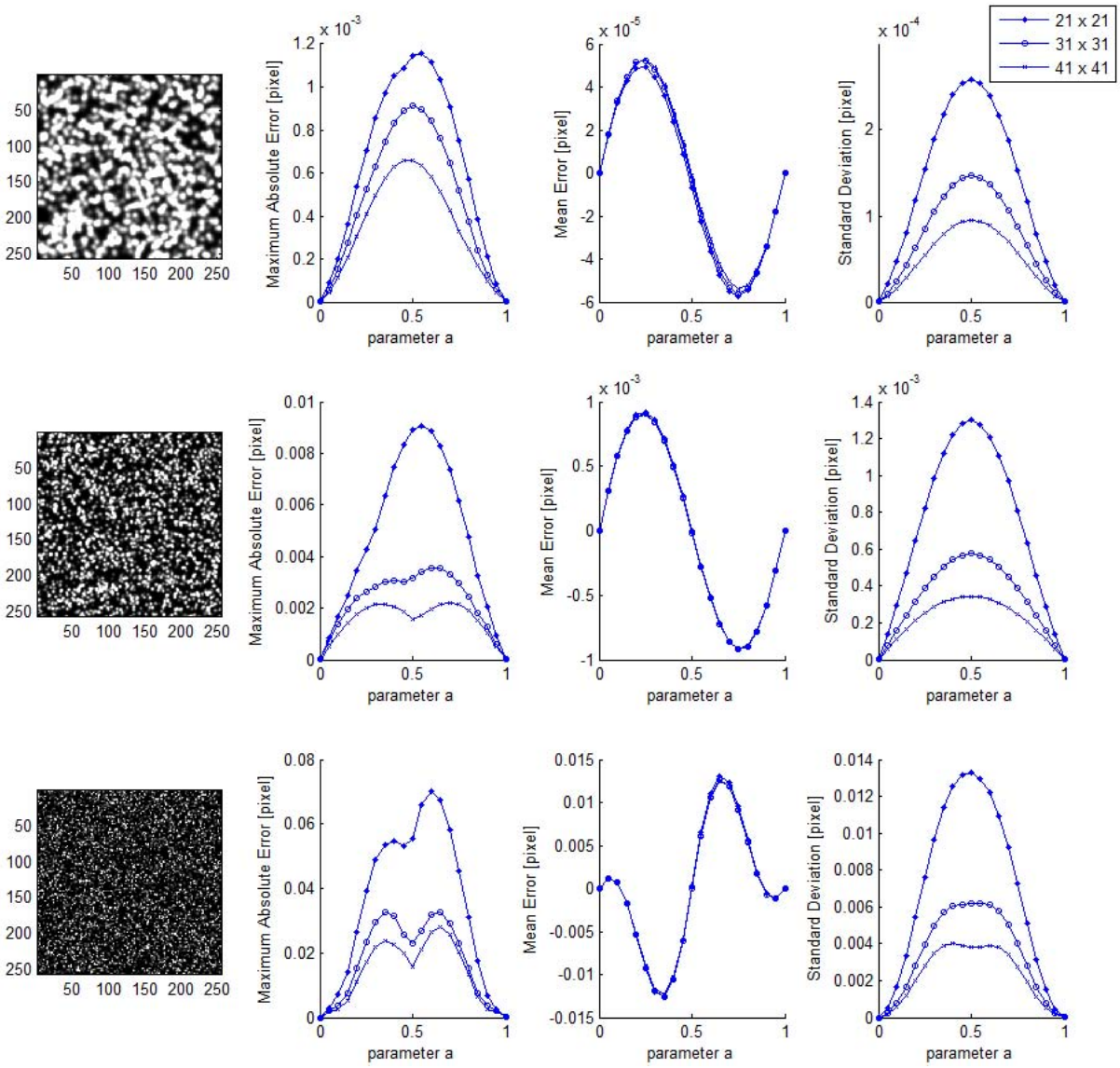

Figure 3: Error results for zero-order displacement field (rigid translation) using different speckle pattern and subset sizes.

4.3 Second-order displacement field

As stated, 11 (eleven) images were generated for the second-order displacement with parameter a ranging from 0 to $a = 0.001$, which implies to a subset stretching of almost 60%. The calculated errors for each one are displayed in Fig. 5. Differently from the previous two cases, the lower absolute error was obtained with the pattern with medium granular size. However, the image with larger pattern presents the lowest absolute error for the highest strain if the smallest subset size is used.

When low strains are imposed for the three patterns, the absolute error decrease when the subset size increase. On the other hand, with large and medium patterns and large strains, the absolute error increases when the subset size increases.

The absolute errors for the larger and medium patterns have comparable values in high strains. Conversely, the mean error is completely different for the three patterns at high strains. These observations suggest that the absolute error may have an exponential growth for with

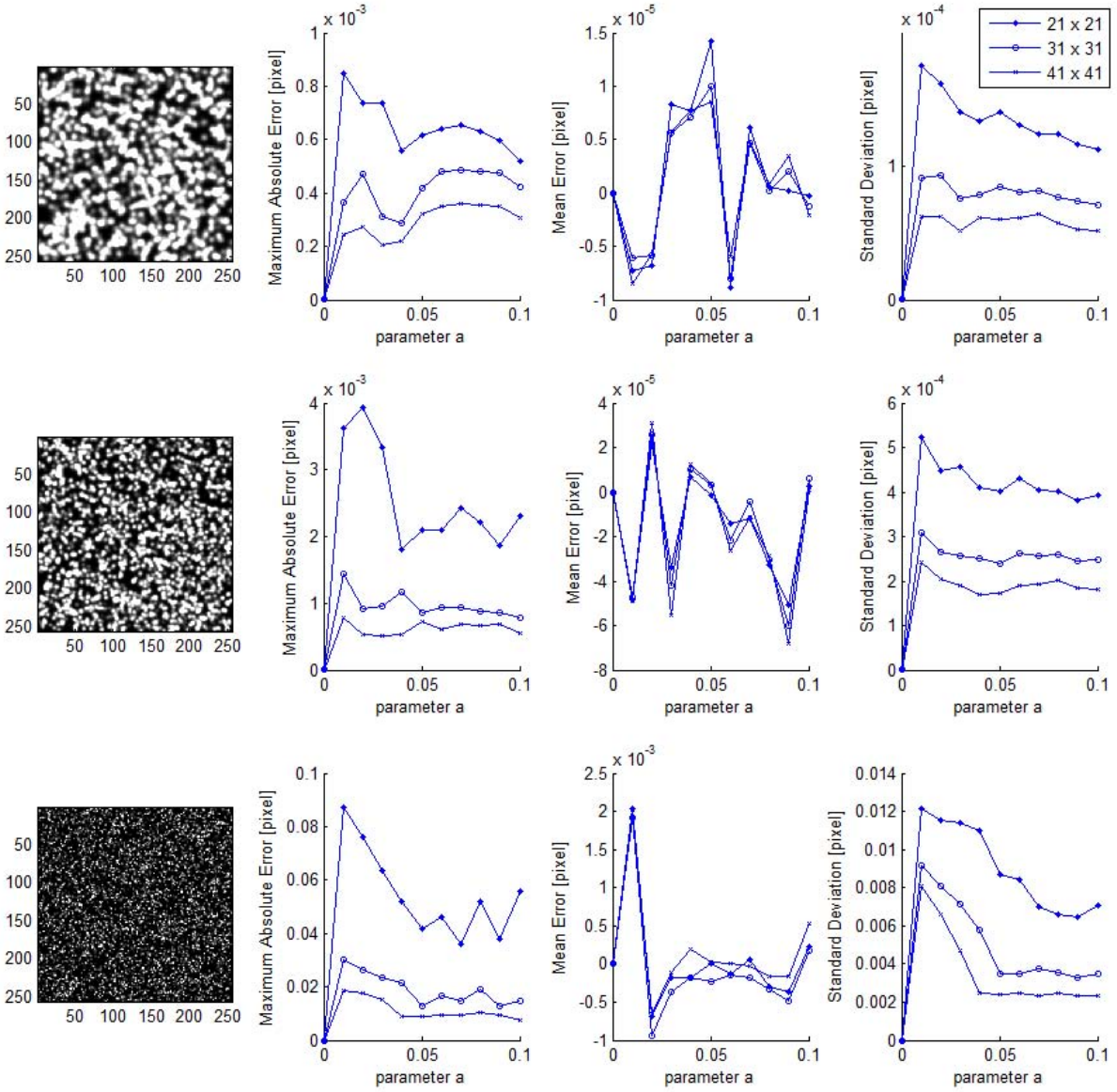

Figure 4: Error results for first-order displacement field using different speckle pattern and subset sizes.

respect to strains due to a no appropriated relationship between the pattern and subset sizes.

The images with the smallest speckle pattern present a maximum absolute error of about 0.075 pixels along the Y-direction of the image obtained with the subset size of 21×21.

The images with large and medium speckle pattern show a maximum absolute error of 0.025 and 0.019 pixels along the Y-direction for a subset size of 41×41. When the subset size is reduced to 21×21 pixels, the images with the largest and medium patterns present a maximum absolute error of 0.004 and 0.0054 pixels respectively. These values are almost one order smaller than the previous case which enforces the strong relationship among subset size, pattern size and characteristics of the displacement field.

5 CONCLUSIONS

It is possible to see that the displacements fields provided by the DIC algorithm closely match the displacements fields numerically generated. However, quite different accuracy may

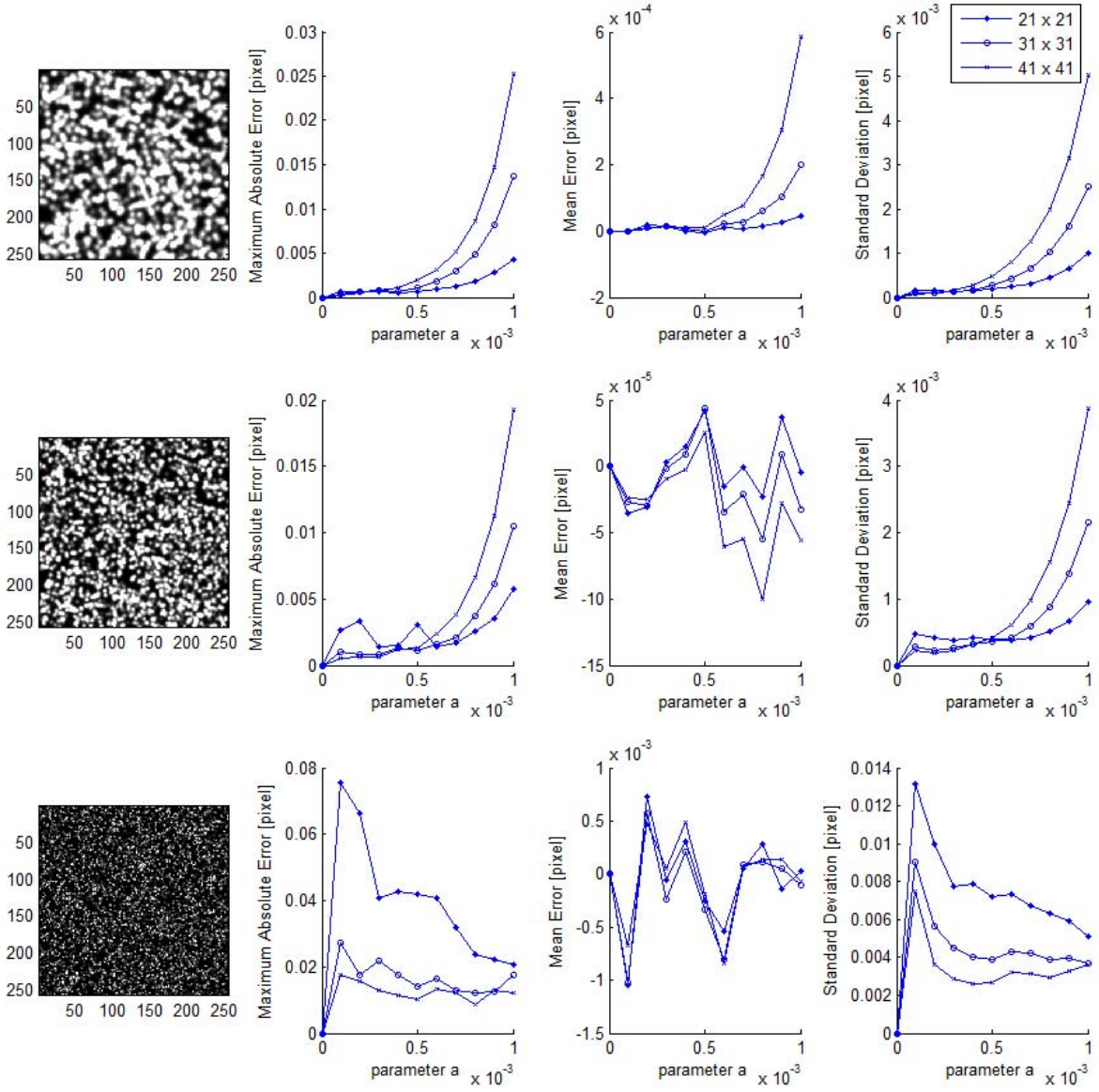

Figure 5: Error results for second-order displacement field using different speckle pattern and subset size.

be obtained depending on important variables that are set up by the user at each particular measurement.

For the set of studied cases it was noted that, in general, the absolute errors for the images with granules with size of about 1 pixel can be quite larger than those obtained with larger granular sizes. The absolute error decreases significantly when the the speckle grows to the size of 4-5 pixels.

For low-order displacement fields (zero and first-order), the absolute error presents better results for large subset sizes. Conversely, small subset sizes have performed better for second-order displacement fields at high strains.

In the identification of mechanical properties, the DIC method has been successful to register accurately the infinitesimal strain at the beginning of the experimental test and also the complex strain field during the necking phenomenon at high strains. In the first images of the sequence, when the specimen presents small displacements, the subset size should be large enough to guarantee high accuracy measurements. Once the necking starts, the the results showed that

smaller subset sizes may be convenient in terms of accuracy.

From the analyzes of different speckle patterns and subset sizes, this work shows the importance of an appropriated relationship between the speckle pattern and the subset size, specially for high-order displacement fields. The results suggest the use of small subset sizes to keep high measurement accuracy for high order displacement fields, but it does not guarantee the best accuracy and precision for low order displacement fields.

To conclude, it is worth noting that although the evidences shown in this work do not offer the ideal speckle granule size or subset size, they emphasize the importance of the choice of these parameters for high-order displacement field. Once this work is focused in the errors related only to the DIC algorithm, it does not mean that the errors associated to the measuring system are less significant. Further studies are needed to investigate other source of errors, like the errors related to real experiments such as noise during acquisition, fluctuation of the illumination, lens distortion and etc.

REFERENCES

Bing P., Hui-min X., Bo-qin X., and Fu-long D. Performance of sub-pixel registration algorithms in digital image correlation. *Measurement Science and Technology*, 17(6):1615–1620, 2006. ISSN 0957-0233. doi:10.1088/0957-0233/17/6/045.

Bruck H., McNeill S., Sutton M., and Peters W. Digital image correlation using newton-raphson method of partial differential correction. *Experimental Mechanics*, 29(3):261–267, 1989.

Guastavino R. and Göransson P. A 3d displacement measurement methodology for anisotropic porous cellular foam materials. *Polymer Testing*, 26(6):711–719, 2007. ISSN 0142-9418. doi:10.1016/j.polymertesting.2007.02.008.

Lecompte D., Smits A., Bossuyt S., Sol H., Vantomme J., Van Hemelrijck D., and Habraken A. Quality assessment of speckle patterns for digital image correlation. *Optics and Lasers in Engineering*, 44(11):1132–1145, 2006. ISSN 0143-8166. doi:10.1016/j.optlaseng.2005.10.004.

Lu H. and Cary P. Deformation measurements by digital image correlation: Implementation of a second-order displacement gradient. *Experimental Mechanics*, 40(4):393–400, 2000.

Pan B., Asundi A., Xie H., and Gao J. Digital image correlation using iterative least squares and pointwise least squares for displacement field and strain field measurements. *Optics and Lasers in Engineering*, 47(7-8):865–874, 2009a. ISSN 0143-8166.

Pan B., Lu Z., and Xie H. Mean intensity gradient: An effective global parameter for quality assessment of the speckle patterns used in digital image correlation. *Optics and Lasers in Engineering*, 48(4):469–477, 2010. ISSN 0143-8166. doi:10.1016/j.optlaseng.2009.08.010.

Pan B., Qian K., Xie H., and Asundi A. Two-dimensional digital image correlation for in-plane displacement and strain measurement: a review. *Measurement Science and Technology*, 20(6):062001–, 2009b. ISSN 0957-0233. doi:10.1088/0957-0233/20/6/062001.

Pan B., Xie H., Wang Z., Qian K., and Wang Z. Study on subset size selection in digital image correlation for speckle patterns. *Optics Express*, 16(10):7037–7048, 2008. doi:10.1364/OE.16.007037.

Schreier H.W., Braasch J.R., and Sutton M.A. Systematic errors in digital image correlation caused by intensity interpolation. *Optical Engineering*, 39(11):2915–2921, 2000. doi:10.1117/1.1314593.

Schreier H.W. and Sutton M.A. Systematic errors in digital image correlation due to undermatched subset shape functions. *Experimental Mechanics*, 42(3):303–310, 2002. doi:10.1007/BF02410987.

Sutton M., McNeill S., Helm J., and Chao Y. *Advances in Two-Dimensional and Three-Dimensional Computer Vision*, volume 77. Springer Berlin, 2000.

Sutton M.A., Orteu J.J., and Schreier H.W. *Image Correlation for Shape, Motion and Deformation Measurements: Basic Concepts, Theory and Applications*. Springer, 2009. doi: 10.1007/978-0-387-78747-3.

Tao G. and Xia Z. A non-contact real-time strain measurement and control system for multi-axial cyclic/fatigue tests of polymer materials by digital image correlation method. *Polymer Testing*, 24(7):844–855, 2005. ISSN 0142-9418. doi:10.1016/j.polymertesting.2005.06.013.

Vanlanduit S., Vanherzeele J., Longo R., and Guillaume P. A digital image correlation method for fatigue test experiments. *Optics and Lasers in Engineering*, 47(3-4):371–378, 2009. ISSN 0143-8166. doi:10.1016/j.optlaseng.2008.03.016.

Vendroux G. and Knauss W. Submicron deformation field measurements: Part 2. improved digital image correlation. *Experimental Mechanics*, 38(2):86–92, 1998.

Zhang D. and Arola D.D. Applications of digital image correlation to biological tissues. *Journal of Biomedical Optics*, 9(4):691–699, 2004. doi:10.1117/1.1753270.